Materials Science & Engineering A 651 (2016) 878–885

Contents lists available at ScienceDirect

Materials Science & Engineering A

journal homepage: www.elsevier.com/locate/msea

A new method for grain refinement in magnesium alloy: High speed extrusion machining

Yao Liu [a,*], Songlin Cai [b], Lanhong Dai [c]

[a] School of Mathematics and Physics, University of Science and Technology Beijing, Beijing 100083, P.R. China
[b] China Electric Power Research Institute, State Grid Corporation of China, Beijing 100192, P.R. China
[c] State Key Laboratory of Nonlinear Mechanics, Institute of Mechanics, Chinese Academy of Science, Beijing 100190, P.R. China

ARTICLE INFO

Article history:
Received 24 September 2015
Received in revised form
15 November 2015
Accepted 16 November 2015
Available online 17 November 2015

Keywords:
High speed extrusion machining
Magnesium alloy
Grain refinement
Dynamic recrystallization

ABSTRACT

Magnesium alloys have received broad attentions in industry due to their competitive strength to density ratio, but the poor ductility and strength limit their wide range of applications as engineering materials. A novel severe plastic deformation (SPD) technique of high speed extrusion machining (HSEM) was used here. This method could improve the aforementioned disadvantages of magnesium alloys by one single processing step. In this work, systematic HSEM experiments with different chip thickness ratios were conducted for magnesium alloy AZ31B. The microstructure of the chips reveals that HSEM is an effective SPD method for attaining magnesium alloys with different grain sizes and textures. The magnesium alloy with bimodal grain size distribution has increased mechanical properties than initial sample. The electron backscatter diffraction (EBSD) analysis shows that the dynamic recrystallization (DRX) affects the grain refinement and resulting hardness in AZ31B. Based on the experimental observations, a new theoretical model is put forward to describe the effect of DRX on materials during HSEM. Compared with the experimental measurements, the theoretical model is effective to predict the mechanical property of materials after HSEM.

© 2015 Elsevier B.V. All rights reserved.

1. Introduction

Weight reduction of automobile is an attractive option for significant advances in both fuel efficiency and the resulting reduction in CO_2 emission [1,2]. Magnesium alloys are attractive metals for the aerospace and automotive field to take advantage of their high strength-to-weight ratio [3]. However, magnesium alloys show poor ductility at ambient temperature due to their hexagonal close-packed (HCP) crystal structure and an insufficient number of operative slips [4]. Compared with the competing materials, the strength of magnesium is lower than that of steel or aluminum [5–7]. Therefore, the poor ductility and strength of magnesium alloys limit their wide range of applications as engineering materials.

Severe plastic deformation (SPD) has emerged as an effective technique to produce ultrafine-grained microstructure for improved ductility and strength [8–11]. Conventional SPD techniques such as equal channel angular pressing (ECAP) [12], high pressure torsion (HPT) [13], accumulative roll bonding (ARB) [14] and accumulative back extrusion (ABE) [15,16] are able to vary the grain size and grain boundary distribution, thus conferring the microstructure significantly different properties. However, in these conventional SPD techniques, multiple passes of deformation process are needed to accumulate large strain in materials, and suitable route and temperature are also necessary in order to refine the microstructure down to ultrafine-grain [17–20].

Machining has been proved to be a particularly effective method to achieve SPD [21,22]. Compared with the conventional SPD techniques, the SPD method of machining needs one deformation step to produce large strain in the material. Chandrasekar and co-workers have used the machining SPD method to promote formation of ultra-fine grained (UFG) and nanocrystalline microstructures [23,24]. In order to control the deformation field, Chandrasekar further devised a large strain extrusion machining (LSEM) apparatus by introducing constraint into machining [25]. Dai and co-workers developed the dynamic LSEM and quasi-static LSEM devices to research the suppression of repeated adiabatic shear banding and deformation field [26,27].

As for the SPD process of magnesium alloy, the SPD speed plays an important role in the deformation behavior of magnesium alloy. Shear bands or crack could be produced at low SPD speed in magnesium alloy [28,29], which is harmful for its usage. As SPD speed increasing, dynamic recrystallization (DRX) behavior is dramatically enhanced by high temperature [28,30]. For low speed

* Corresponding author.
E-mail address: liuyao@ustb.edu.cn (Y. Liu).

http://dx.doi.org/10.1016/j.msea.2015.11.046
0921-5093/© 2015 Elsevier B.V. All rights reserved.

LSEM magnesium alloys, Efe et al. first suppressed the crack initiation in magnesium alloy sheet by high hydrostatic pressure [29]. However, high speed LSEM magnesium alloys is not explored in improving the properties of magnesium alloys. It is suggested that remarkable grain refinement could be obtained during high speed LSEM magnesium alloys, due to the contribution of DRX in high speed SPD. Grain refinement could potentially help to improve strength of magnesium alloys owing to Hall–Petch relationship [31,32]. Therefore, it is meaningful to research the grain refinement of magnesium alloys in high speed extrusion machining (HSEM).

In this paper, in order to enhance DRX behavior, a high speed LSEM device is designed to process magnesium alloys. A systematic HSEM experiments with different chip thickness ratios were conducted for magnesium alloy. The cutting speed is 10 m/s. The chip morphology reveals the variation of microstructure in magnesium alloy with decreasing chip thickness ratio. Compared with the microstructure in magnesium alloy before HSEM experiments, the grains after HSEM experiments are refined more greatly. There are multiple grain sizes for large chip thickness ratio in HSEM, where the large grains are surrounded by smaller grains. With the decreasing chip thickness ratio, the large grains are further refined and uniformly small grains are attained. To characterize the mechanical property of magnesium alloy for different chip thickness ratios in HSEM, Vickers hardness testing of magnesium alloy is conducted before and after HSEM. The Vickers hardness measurements show that the magnesium alloys of multiple grain sizes have a better mechanical property than that of the uniformly small grains.

The paper is organized as follows: in Section 2 we briefly narrate the experimental procedure of the HSEM magnesium alloy AZ31B. The microstructural observations and the mechanical properties of magnesium alloys for different chip thickness ratios are given in Section 3. Section 4 presents the theoretical model for HSEM magnesium alloys. Section 5 gives remarkable conclusions of our present investigation.

2. Experimental procedure

The initial sample used in the experiments is magnesium alloy plate AZ31B. Chemical composition is specified in Table 1. The annealing temperature of AZ31B is 345 °C. The microstructure of the initial sample and its grain size distribution are illustrated in Fig. 1. The average initial grain size is about 38.9 μm as shown in Fig. 1b.

The technique of HSEM has been elaborated in [27]. Fig. 2 shows a schematic of HSEM, where an orthogonal machining process is taken into consideration. The wedge-shaped tool with a rake angle α is static and the workpiece with a cutting layer depth t_0 is moving toward the tool. Finally, because of the process of shear in primary shear zone (PSZ) OA, the workpiece materials in the cutting layer flow out along the rake face of the tool in the form of a chip with a thickness t_c. The inclined angle φ of PSZ is named as shear angle. Based on the definition of chip thickness ratio $\lambda = t_c/t_0$ [33,34], the different chip thickness ratios can be obtained by changing the position of constraint during HSEM.

In order to explore the relationship between different chip thickness ratios and microstructure of magnesium alloy in HSEM, the different cutting conditions for HSEM AZ31B are listed in Table 2 by adjusting the position of constraint. After cutting, chips were collected and embedded into clean resin. The lateral process was mechanically polished and then the polished surfaces were etched in a 5 g picric acid + 10 ml water + 10 ml acetic acid + 100 ml ethanol solution for about 10 s to reveal the deformed microstructure of AZ31B.

Table 1
Chemical composition of the magnesium alloy AZ31B.

Elements	Mg	Al	Zn	Mn	Si	Cu	Ca	Others
Wt. (%)	97	2.5–3.5	0.6–1.4	0.2	0.1	0.05	0.04	≤0.01

These etched specimens were further observed with the optical microscope (Olympus BX51M) to examine the morphologies of chips. The grain sizes were measured by the planimetric procedure in the image analysis software Image Pro-Plus 6.0 according to ASTM E112-10 method by counting at least 500 grains [35,36].

The specimens for electron backscatter diffraction (EBSD) analysis were prepared by polishing with SiC (down to 2000 grit size) and further electropolishing using a solution of 90 ml ethanol and 10 ml perchloric acid (25 V at −30 °C). JOEL JSM-7800F was used to examine EBSD maps of AZ31B samples. The operating voltage was 15 KV and the observation surface was on the cross section perpendicular to normal direction (ND). The scanning step length was 2 μm and 0.4 μm for the initial sample and deformed samples respectively.

Vickers hardness testing of samples is further conducted on the hardness tester (Everone MH-5L) to reveal the relationship between the mechanical property and the microstructure of magnesium alloy. Vickers hardness measurements were carried out on the cross section perpendicular to ND at regular distance intervals, using a 100 g load for 15 s.

3. Experimental observations

3.1. Microstructure measurements

Fig. 3 shows the microstructure of chips for different chip thickness ratios in HSEM AZ31B under the cutting condition of Table 2. Compared Fig. 1 with Fig. 3, the originally coarse grains are refined more markedly by even a single pass of HSEM processing. The chip thickness ratio in HSEM has a great influence on grain refinement. The grains have a heterogeneous distribution in HSEM for large chip thickness ratio where the large grains are surrounded by smaller grains (Fig. 3a). With the decreasing chip thickness ratio, the large grains are further refined and the small grains have a homogeneous distribution in chips (Fig. 3b–d).

In order to reveal the relationship between grain size and chip thickness ratio, the grain sizes were measured by the statistical methods described in experimental procedure and the distribution of grain sizes is illustrated in Fig. 4. The grains of the AZ31B before HSEM have a Gaussian distribution with the average grain size of 38.9 μm (Fig. 1). Compared with the initial grain size, the average grain size of AZ31B after HSEM is much smaller.

The grains are refined by controlled chip thickness ratio in HSEM; however, the grain size distribution varies with chip thickness ratio. For the chip thickness ratio $\lambda = 0.93$ (Fig. 4a), the grains have a heterogeneous distribution with grain size ranging from 0.5 μm to 50 μm and a bimodal grain structure of coarse grains embedded in a fine matrix is produced. About 70% of the microstructure is composed of fine grains with a mean size of 2 μm, while the rest of the grains have sizes ranging from 8 μm up to 50 μm. When the chip thickness ratio is less than a certain value (Fig. 4b–d), the bimodal grain size distribution disappear and the refined grains have a Gaussian distribution. As shown in Fig. 4b–d, the average grain sizes for $\lambda = 0.57$, $\lambda = 0.43$ and $\lambda = 0.32$ are close to each other. The chip thickness ratio less than a certain value can not remarkably affect the grain refinement if the initial temperature and cutting speed are both fixed in HSEM.

It is noteworthy that the average grain size can be refined down to ~2 μm in HSEM at the ambient temperature of 293 K by a

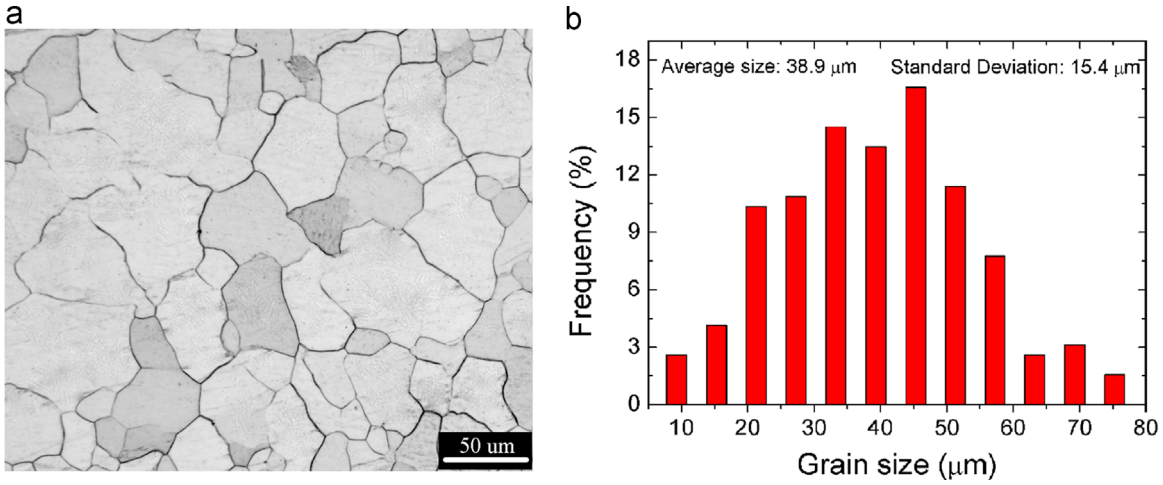

Fig. 1. (a) The initial microstructure of AZ31B at the normal direction (ND); (b) the initial grain size distribution.

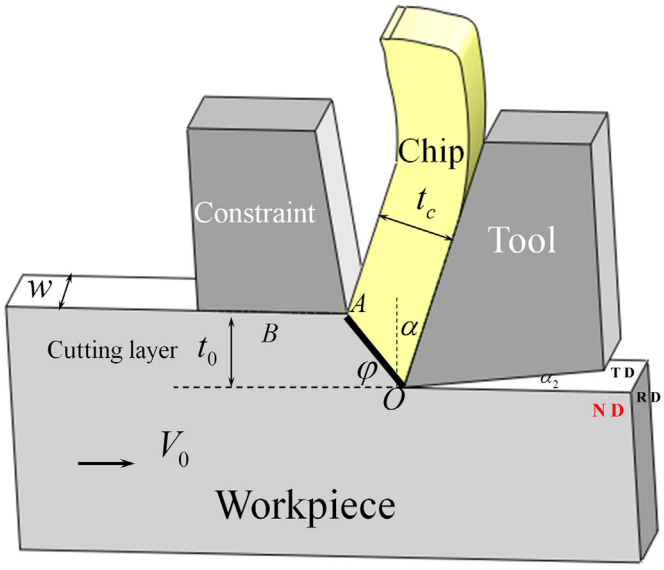

Fig. 2. Schematic of high speed extrusion machining (HSEM) where the relevant parameters are denoted.

Table 2
Cutting condition in HSEM AZ31B.

Cutting parameters	Notation	Value
Rake angle	α	10°
Clearance angle	α_2	5°
Precut chip thickness	t_0	200 μm
Cutting width	w	5 mm
Cutting speed	V_0	10 m/s
Controlled chip thickness	t_c	186, 114, 86, 64 μm
Chip thickness ratio	λ	0.93, 0.57, 0.43, 0.32

single pass of deformation process, which is comparable to the value of 2 μm after four-pass ABE at the temperature of 503 K [15] and is even less than that of 5.5 μm for AZ31 alloy produced by eight-pass ECAP at the temperature of 523 K [17]. Jorge et al. processed AZ31 alloy by ECAP under conditions of temperature and numbers of passes in order to avoid grain growth [37]. In their experiments [37], AZ31 alloy was processed by two-pass ECAP at 473 K and a subsequent two-pass ECAP at 443 K, which leads to an average grain size less than 1 μm. Both ABE and ECAP need multiple passes of deformation process to refine the grains down to 2 μm or less than 1 μm. Although HSEM and integrated forward extrusion and torsion [38] are both a single pass of deformation process, the grain size for small chip thickness ratio in HSEM is more homogeneous than that after integrated forward extrusion and torsion at high temperature. Thus, HSEM is an effective method for attaining the homogeneous and refined grains.

In order to explore the variation of texture during HSEM, the AZ31B samples with different chip thickness ratios were further characterized by EBSD technique. The orientation imaging maps (OIM) for AZ31B samples before HSEM and after HSEM with different chip thickness ratios are shown in Fig. 5. The strong basal textures ({0001}‖ND) are observed in each samples. With the decreasing chip thickness ratio, crystal orientations with {0001}⊥ND are gradually increased. The crystal orientation change results from the recrystallization during HSEM, which makes the basal texture ({0001}‖ND) slightly weakened. Fig. 6 illustrates the pole figures (PF) of AZ31B before HSEM and after HSEM. The texture of the initial AZ31B is a typical basal texture with a relatively stronger intensity (see in Fig. 6a), where the (0001) poles are oriented parallel to the ND of the sample. As shown in Fig. 6b–c, the textures after HSEM are different from the basal texture of the initial AZ31B. The chips after HSEM exhibits tilted-basal texture components wherein the basal planes are tilted from the sample surface. The tilted-basal texture components for $\lambda = 0.93$ and $\lambda = 0.43$ have the basal poles inclined away from ND towards RD by ~30 °and ~23 ° respectively. Compared with the intensity at higher λ, the tilted-basal texture at smaller λ has a weaker intensity. It is indicated that the basal texture weakens with the decreasing chip thickness ratio in HSEM.

3.2. Hardness measurements

The mechanical property of materials is related with the microstructure in materials [39,40]. Different microstructures may lead to the variation of mechanical property. Vickers hardness testing is conducted before and after HSEM to research the mechanical property of AZ31B which is produced by SPD method of HSEM. The Vickers hardness measurements of AZ31B before and after HSEM are depicted in Fig. 7. As seen in Fig. 7, Vickers hardness of AZ31B in HSEM decreases with the decreasing chip thickness ratio. Compared with the Vickers hardness of AZ31B before HSEM, the Vickers hardness for $\lambda = 0.93$ in HSEM increases nearly by 36%. The Vickers hardness for $\lambda = 0.57$ in HSEM increases by 22%. For $\lambda = 0.43$ or $\lambda = 0.32$ in HSEM, however, the Vickers hardness is close to that of AZ31B before HSEM. Therefore, the SPD method of HSEM is efficient to improve the mechanical property of materials by controlling the chip thickness ratio in HSEM.

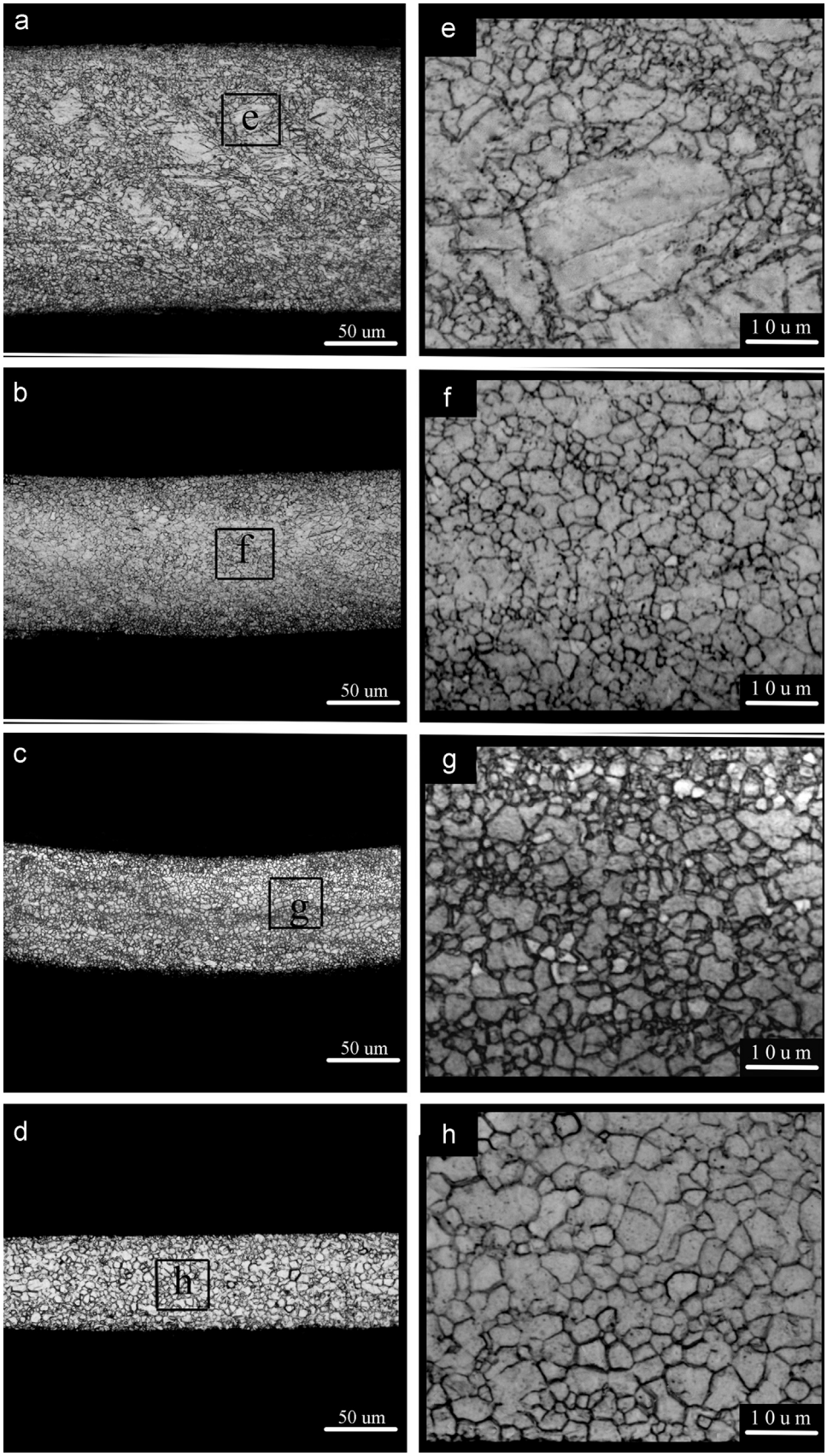

Fig. 3. Microstructural observations of chips for different chip thickness ratios in HSEM: (a) $\lambda = 0.93$; (b) $\lambda = 0.57$; (c) $\lambda = 0.43$; (d) $\lambda = 0.32$; (e), (f), (g) and (h) are the local magnifications of (a), (b), (c) and (d) respectively.

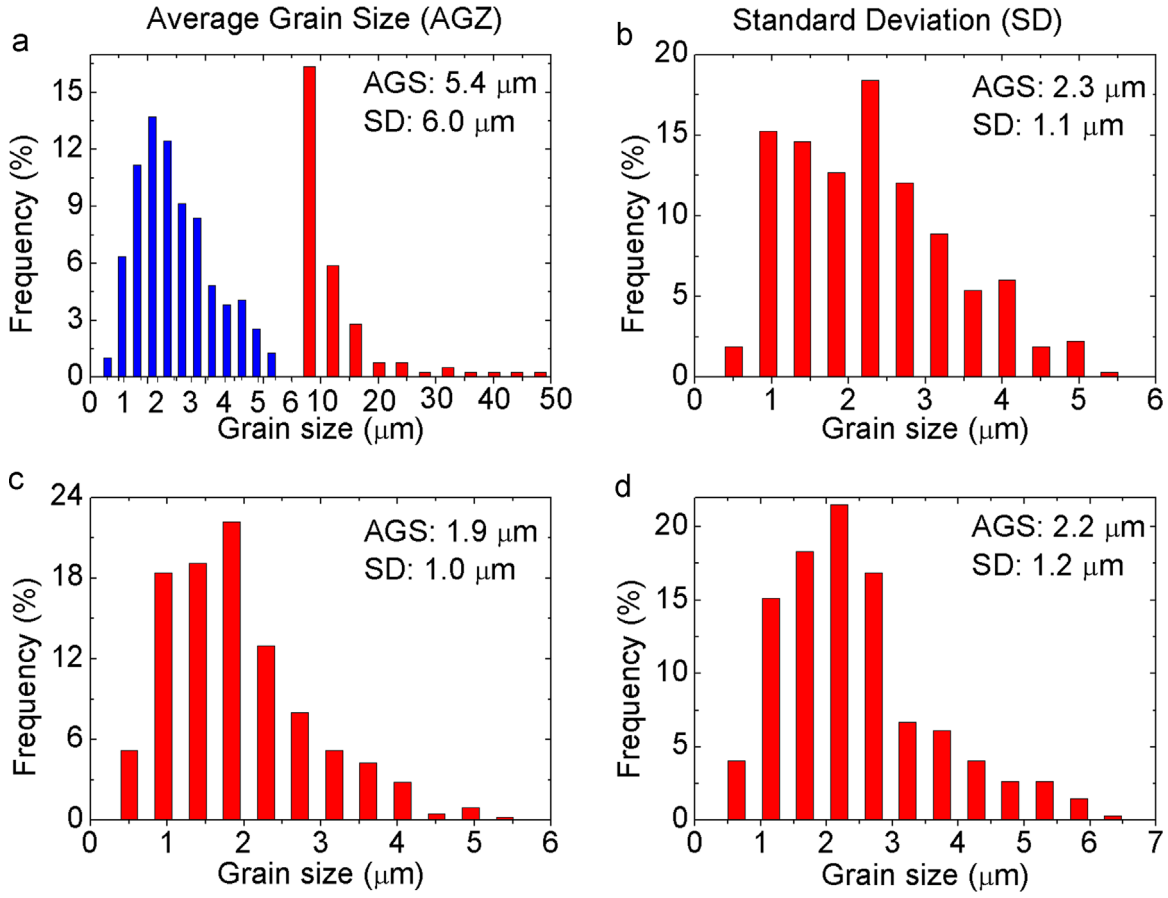

Fig. 4. Grain size distribution of AZ31B after HSEM: (a) $\lambda = 0.93$; (b) $\lambda = 0.57$; (c) $\lambda = 0.43$; (c) $\lambda = 0.32$.

For $\lambda = 0.93$ in HSEM, we also identified many tinny grains of ~2 μm and some large elongated grains of 10–50 μm (Fig. 4a), suggesting that the DRX does not take place completely. However, for $\lambda = 0.57$ or $\lambda = 0.43$ in HSEM, the uniformly tinny grains of ~2 μm are attained, indicating that the DRX for all the originally coarse grains take place fully. Based on the shear strain formula in extrusion machining [33,34,41], the shear strain γ in PSZ is given by:

$$\gamma = \frac{\lambda}{\cos\alpha} + \frac{1}{\lambda\cos\alpha} - 2\tan\alpha. \quad (1)$$

Substituting the values of machining parameters λ and α into Eq. (1), the shear strains in Fig. 3a–d are 1.68, 2.01, 2.45 and 3.04 respectively. Compared with the shear strains in Fig. 3b–d, the incomplete DRX in Fig. 3a can be attributed to the lower shear strain. The combination of complete and incomplete DRX grains for $\lambda = 0.93$ in HSEM is favorable for the improvement of Vickers hardness. With the decreasing chip thickness ratio, the larger

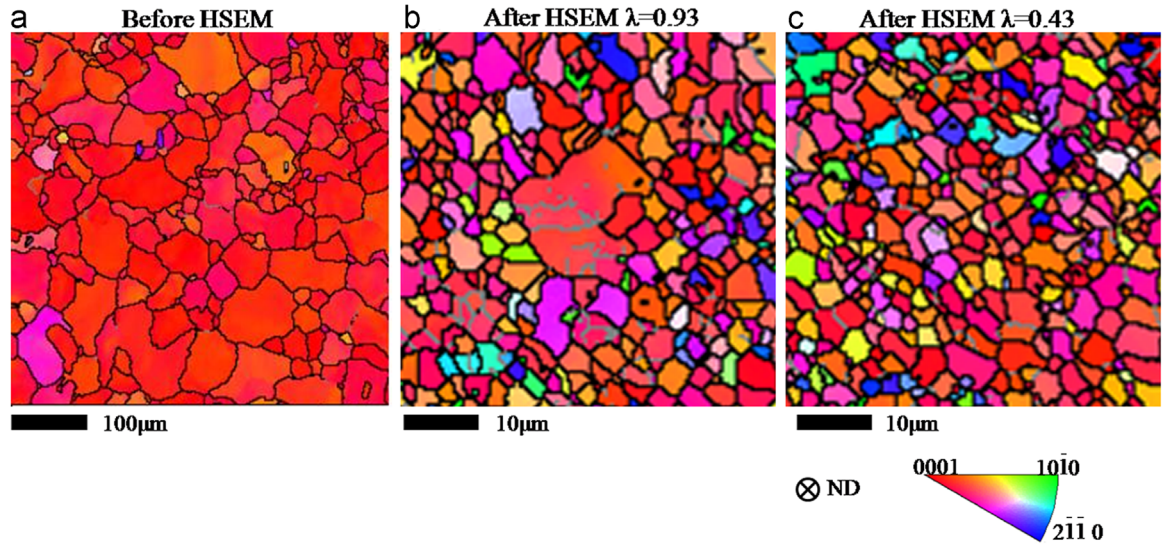

Fig. 5. The orientation imaging maps (OIM) for magnesium alloy samples (a) before HSEM, (b) after HSEM λ=0.93, and (c) after HSEM λ=0.43.

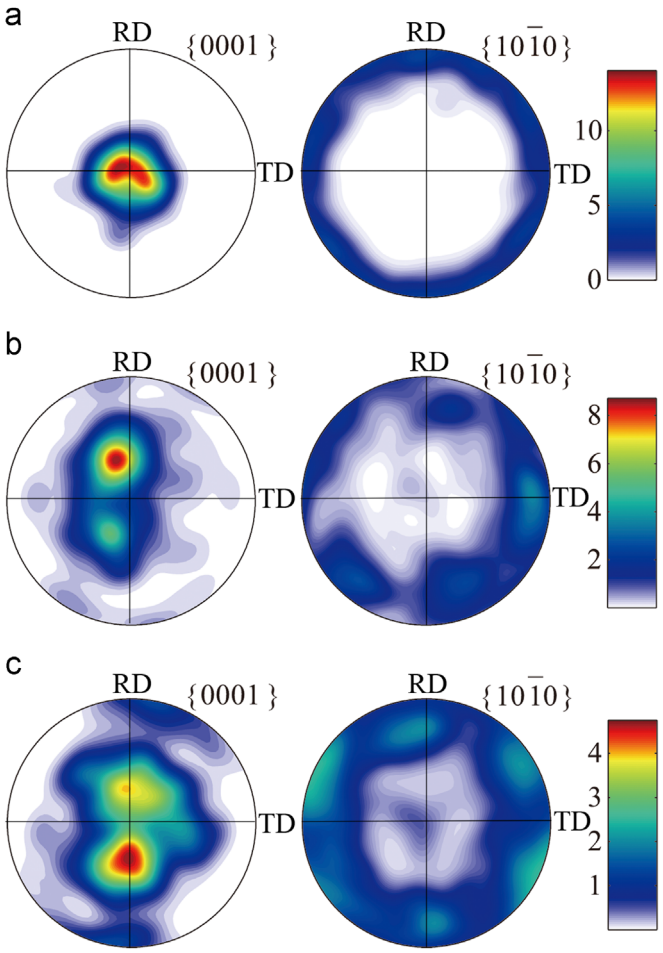

Fig. 6. The pole figures (PF) for magnesium alloy samples (a) before HSEM, (b) after HSEM λ=0.93, and (c) after HSEM λ=0.43.

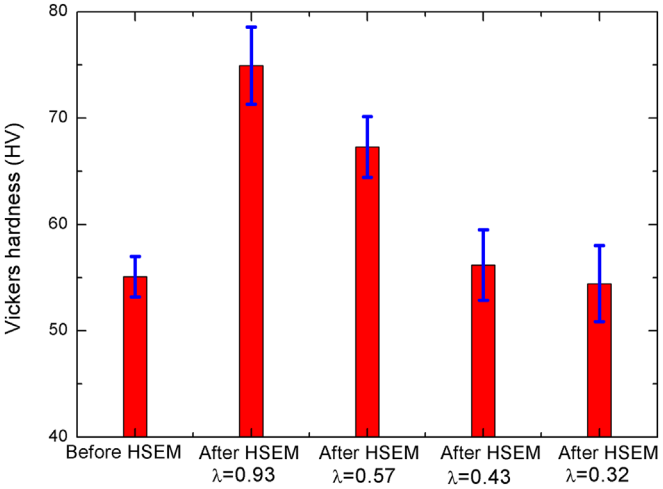

Fig. 7. Vickers hardness measurements of AZ31B before and after HSEM for different chip thickness ratios.

shear strain in Fig. 3b–d induces a full DRX for the elongated grains. The grains are homogeneously refined to about 2 μm (Fig. 4b–d) due to the complete DRX. During the complete DRX, the dislocations that generate due to SPD are incorporated by the transformation of low angle boundaries (LABs) to high angle boundaries (HABs) [15]. The complete DRX in chips with small chip thickness ratio may absorb the dislocations which are emitted due to large strain in HSEM, thus, the Vickers hardness does not increase any more though the grains are homogeneously refined down to 2 μm.

4. Theoretical model

The yield strength of AZ31B magnesium alloy before HSEM is assumed to be σ_0, but the yield strength after HSEM σ_Y can be increased because severe plastic deformation (SPD) is imposed on AZ31B alloy during HSEM. According to the Taylor equation [42,43], the yield stress σ_Y is given by:

$$\sigma_Y = \sigma_0 + \beta MGb\sqrt{\rho}, \tag{2}$$

where G is the shear modulus, β is a numerical constant which depends on the strength of the dislocation–dislocation interaction, M is the Taylor factor, b is the magnitude of the Burgers vector and ρ is the dislocation density due to SPD in HSEM.

Because DRX occurs in HSEM, the dislocation density ρ contains two parts: the dislocation density in grains of no DRX ρ_n and the dislocation density in DRX grains ρ_s. The volume fraction of DRX X_D ($0 \le X_D \le 1$) is introduced here to describe the degree of DRX. There are no DRX for $X_D = 0$ and complete DRX for $X_D = 1$ in materials; otherwise, the incomplete DRX happens in materials. The dislocation density ρ in HSEM is determined by the following form:

$$\rho = \rho_n(1 - X_D) + \rho_s X_D. \tag{3}$$

The dislocation density ρ_n in the DRX-free grains increases with the deformation during HSEM; however, the dislocation density ρ_s in DRX grains is low because DRX absorbs the increasing dislocation density resulting from SPD. According to the Kocks–Mecking–Estrin (KME) model [44–47], the evolution of dislocation density ρ_n in the DRX-free grains is given by:

$$\frac{d\rho_n}{d\varepsilon} = M\left(\frac{1}{b\Lambda} + k_1\sqrt{\rho_n} - k_2\rho_n\right). \tag{4}$$

In Eq. (4), ε is the effective strain which is equal to $\gamma/\sqrt{3}$, Λ is determined by grain size, the coefficient k_1 and k_2 represent the dislocation storage rate and the dynamic recovery rate. The initial dislocation density for $\varepsilon = 0$ is assumed to be ρ_0 in order to solve Eq. (4).

The DRX kinetics model of magnesium alloy AZ31B proposed by Liu [48] is as follows:

$$\ln\left(\frac{1 - X_D}{X_D}\right) = \left(1 - \frac{\varepsilon - \varepsilon_c}{\varepsilon_{0.5} - \varepsilon_c}\right)\ln K_v, \tag{5}$$

where K_v is a constant decided by the initial grain size and the stacking-fault energy, ε_c is the critical strain and $\varepsilon_{0.5}$ is the strain for 50% DRX. The critical strain ε_c and the strain for 50% DRX $\varepsilon_{0.5}$ can be rewritten as the function of the Zener–Hollomon parameter Z [48]:

$$\varepsilon_c = 0.0061Z^{0.1029}, \tag{6}$$

$$\varepsilon_{0.5} = 0.0426Z^{0.0781}. \tag{7}$$

The parameter Z is given by the Arrhenius equation [49]:

$$Z = \dot{\varepsilon}\exp\left(\frac{Q}{RT}\right), \tag{8}$$

where $\dot{\varepsilon}$ is the effective strain rate, R is the universal gas constant, Q is the activation energy for deformation, T is the absolute temperature. The effective strain rate $\dot{\varepsilon}$ is in the following form [50,51]:

$$\dot{\varepsilon} = \frac{V_0 \cos\alpha}{\sqrt{3}h\cos(\varphi-\alpha)}. \tag{9}$$

The parameter h in Eq. (9) is the thickness of primary shear zone (PSZ), which is assumed to be $t_0/10$ in the literatures [52–54].

In order to calculate the temperature T during HSEM, the research results of Efe et al. [29] are used here:

$$T = \frac{(1-\Gamma)u_s}{\rho_m c} + T_a, \tag{10}$$

$$\Gamma = \frac{1}{4Y}erf\left(\sqrt{Y}\right) + (1+Y)erfc\left(\sqrt{Y}\right) - \frac{e^{-Y}}{\sqrt{\pi}}\left(\frac{1}{2\sqrt{Y}} + \sqrt{Y}\right), \tag{11}$$

$$Y = \frac{\rho_m c V_0 t_0 \cos\alpha}{4k(\lambda - \sin\alpha)}, \tag{12}$$

where ρ_m is the density of AZ31B, c is the special heat, k is the thermal conductivity, Γ is the fraction of shear plane heat flowing into the workpiece, T_a is the initial workpiece temperature and u_s is the energy per unit volume dissipated at the shear plane. The work has shown that u_s increases from 2.3×10^8 to 4.3×10^8 J/m^3 when λ is decreased from 1.4 to 0.7 [29].

Substituting the parameter values in Tables 2 and 3 into Eqs. (10)–(12), the relationship between the temperature T and cutting speed V_0 is illustrated in Fig. 8. The temperature T increases monotonically with the cutting speed V_0 and reaches a nearly constant at high speeds. The temperature T increases with the decreasing chip thickness ratio λ due to the increasing deformation level. As shown in Fig. 8, the temperature in AZ31B during HSEM can reach up to 509 K at the cutting speed of 10 m/s without pre-heating the workpiece.

For a given cutting speed V_0, numerical analysis of Eqs. (2)–(12) can characterize the yield stress σ_Y of AZ31B after HSEM. According to the research results of Khodabakhshi and co-workers [55], the relationship between hardness and strength in SPD metals can be presented as follow:

$$H_V = \frac{\sigma_Y}{3}(0.1)^{-n}, \tag{14}$$

where H_V is the Vickers hardness, and n is the work hardening exponent.

Table 3
Material parameters for AZ31B.

Parameters	Notation	Value
Shear modulus	G	17 GPa
Material density	ρ_m	1700 kg/m^3
Special heat	c	1000 J/(kg·K)
Thermal conductivity	k	96 w/(m·K)
Initial workpiece temperature	T_a	300 K
Dislocation density in DRX grains	ρ_s	5×10^{13}m^{-2}
Taylor factor	M	3.06
Magnitude of Burgers vector	b	1.29×10^{-10}m
Grain size	Λ	$1.9\text{–}5.4\times10^{-6}$m
Dislocation storage rate	k_1	1.4×10^8m^{-1}
Dynamic recovery rate	k_2	6.5
Initial dislocation density before HSEM	ρ_0	5×10^{13}m^{-2}
Coefficient in Eq. (5)	K_v	150
Activation energy	Q	132 KJ/mol
Universal gas constant	R	8.31 J/(mol·K)
Melting temperature	T_m	820 K
Coefficient in Eq. (2)	β	0.3
Initial yield stress before HSEM	σ_0	110 MPa
Work hardening exponent	n	0.12

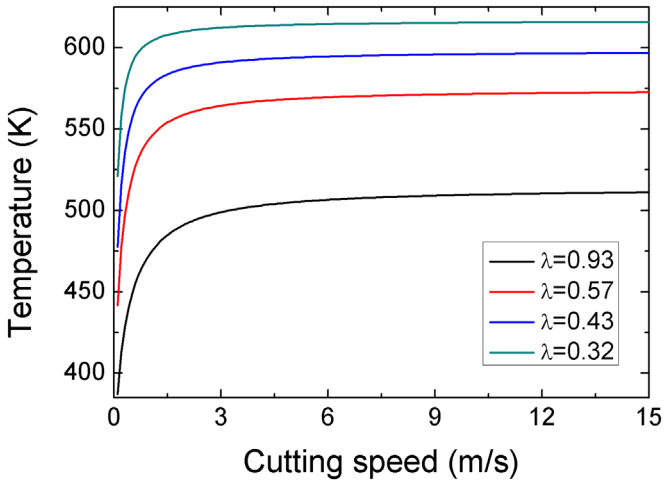

Fig. 8. Variation of temperature with cutting speed for different chip thickness ratios.

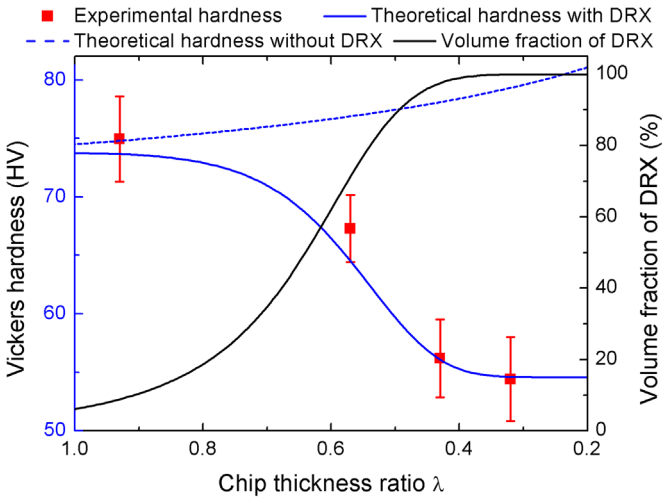

Fig. 9. Comparison of theoretical results with experimental measurements.

Solving the Eqs. (1)–(14) under the cutting parameters in Table 2 and the material parameters in Table 3, the relationship between Vickers hardness H_V and chip thickness ratio λ is shown in Fig. 9, where the variation of DRX volume fraction with chip thickness ratio is also depicted. In order to reveal how DRX affacts the deformation process in HSEM, the comparison between theoretical model with DRX and that without DRX is illustrated in Fig. 9. For larger chip thickness ratio ($\lambda > 0.8$), the volume fraction of DRX is less than 15%, which leads to a great increase of hardness during HSEM. However, for smaller chip thickness ratio ($\lambda < 0.5$), the complete DRX takes place in HSEM, which results in the decrease of dislocation density and finally has an adverse effect on hardness. When the chip thickness ratio is larger than 0.5 and smaller than 0.8, it is a transition state where the hardness has a medium value. As shown in Fig. 9, the theoretical results with DRX are in good accordance with the experimental measurements. If DRX is not taken into consideration in the theoretical model, the theoretical hardness without DRX increases with the decreasing λ (dash line in Fig. 9), which obviously deviates from the experimental results at smaller λ. Compared with the theoretical model without DRX and experimental measurements, the theoretical model with DRX is valid to predict the mechanical property after HSEM.

5. Concluding remarks

In summary, a novel severe plastic deformation (SPD) technique of high speed extrusion machining (HSEM) was used to improve the mechanical property of magnesium alloys. Using the high speed extrusion machining (HSEM) technique, systematic experiments of magnesium alloy AZ31B were conducted with different chip thickness ratios at the cutting speed of 10 m/s. The microscopic observations of chips reveal that HSEM is an effective SPD method for refining the grains and weakening the texture. The different microstructures in magnesium alloy can be attained by controlling the chip thickness ratio in HSEM, leading to a different mechanical property.

A bimodal grain structure of coarse grains embedded in a fine matrix is produced for large chip thickness ratio in HSEM. However, with the decreasing chip thickness ratio, refined grains with a Gaussian distribution are obtained. The EBSD measurements show that the bimodal grain structure results from the incomplete DRX, while the complete DRX leads to the refined grains with a Gaussian distribution. The Vickers hardness in the magnesium alloys with a bimodal grain structure increases by 31%, while that in the magnesium alloys with a refined microstructure barely increases. We attribute this phenomenon to the incorporation of dislocation during the process of the complete DRX.

Based on the experimental observations, a theoretical model is put forward where dislocation storage, dynamic recovery of dislocation and incorporation of dislocation due to DRX are included. The theoretical predictions are in good agreement with the experimental results. Therefore, the theoretical model is valid to predict the mechanical property of materials after HSEM.

Acknowledgments

This work has been supported by the National Natural Science Foundation of China (Grant no. 11132011), Fundamental Research Funds for the Central Universities (Grant no. FRF-TP-15-101A1), the National Basic Research Program of China (Grant no. 2012CB937500), and the CAS/SAFEA International Partnership Program for Creative Research Teams.

References

[1] F.K. Abu-Farha, M.K. Khraisheh, J. Mater. Eng. Perform. 16 (2007) 192–199.
[2] A.S. Khan, A. Pandey, T. Gnäupel-Herold, R.K. Mishra, Int. J. Plast. 27 (2011) 688–706.
[3] M. Janeček, M. Popov, M.G. Krieger, R.J. Hellmig, Y. Estrin, Mater. Sci. Eng. A 462 (2007) 116–120.
[4] T. Al-Samman, G. Gottstein, Mater. Sci. Eng. A 488 (2008) 406–414.
[5] M. Eddahbi, J.Ad Valle, M.T. Pérez-Prado, O.A. Ruano, Mater. Sci. Eng. A 410–411 (2005) 308–311.
[6] B.L. Mordike, T. Ebert, Mater. Sci. Eng. A 302 (2001) 37–45.
[7] Y. Liu, Y. Wei, Int. J. Plast. 55 (2014) 80–93.
[8] R.Z. Valiev, R.K. Islamgaliev, I.V. Alexandrov, Prog. Mater. Sci. 45 (2000) 103–189.
[9] M. Furukawa, Z. Horita, T.G. Langdon, Mater. Sci. Eng. A 332 (2002) 97–109.
[10] R.Z. Valiev, Adv. Eng. Mater. 5 (2003) 296–300.
[11] V. Sklenicka, J. Dvorak, P. Kral, M. Svoboda, M. Kvapilova, T.G. Langdon, Mater. Sci. Eng. A 558 (2012) 403–411.
[12] V.M. Segal, V.I. Reznikov, A.E. Drobyshevskiy, V.I. Kopylov, Russ. Metall. 1 (1981) 99–105.
[13] N.A. Smirnova, V.I. Levit, V.I. Pilyugin, R.I. Kuznetsov, L.S. Davydova, V. A. Sazonova, Fiz. Met. Metalloved. 61 (1986) 1170–1177.
[14] N. Tsuji, Y. Saito, S.H. Lee, Y. Minamino, Adv. Eng. Mater. 5 (2003) 338–344.
[15] S.M. Fatemi-Varzaneh, A. Zarei-Hanzaki, J.M. Cabrera, P.R. Calvillo, Mater. Chem. Phys. 149–150 (2015) 339–343.
[16] S.M. Fatemi-Varzaneh, A. Zarei-Hanzaki, Mater. Sci. Eng. A 528 (2011) 1334–1339.
[17] S. Seipp, M.F.X. Wagner, K. Hockauf, I. Schneider, L.W. Meyer, M. Hockauf, Int. J. Plast. 35 (2012) 155–166.
[18] W.J. Kim, S.W. Chung, C.S. Chung, D. Kum, Acta Mater. 49 (2001) 3337–3345.
[19] E. Mostaed, A. Fabrizi, D. Dellasega, F. Bonollo, M. Vedani, J. Alloy. Compd. 638 (2015) 267–276.
[20] Z.S. Levin, K. Ted Hartwig, Mater. Sci. Eng. A 635 (2015) 94–101.
[21] A.P. Zhilyaev, A.A. Gimazov, G.I. Raab, T.G. Langdon, Mater. Sci. Eng. A 486 (2008) 123–126.
[22] N. Ahmed, A.V. Mitrofanov, V.I. Babitsky, V.V. Silberschmidt, Mater. Sci. Eng. A 424 (2006) 318–325.
[23] S. Swaminathan, T.L. Brown, S. Chandrasekar, T.R. McNelley, W.D. Compton, Scr. Mater. 56 (2007) 1047–1050.
[24] S. Swaminathan, M.R. Shankar, S. Lee, J. Hwang, A.H. King, R.F. Kezar, B.C. Rao, T.L. Brown, S. Chandrasekar, W.D. Compton, K.P. Trumble, Mater. Sci. Eng. A 410–411 (2005) 358–363.
[25] T.L. Brown, C. Saldana, T.G. Murthy, J.B. Mann, Y. Guo, L.F. Allard, A.H. King, W. D. Compton, K.P. Trumble, S. Chandrasekar, Acta Mater. 57 (2009) 5491–5500.
[26] S.L. Cai, Y. Chen, G.G. Ye, M.Q. Jiang, H.Y. Wang, L.H. Dai, J. Mater. Process. Technol. 216 (2015) 48–58.
[27] S.L. Cai, L.H. Dai, J. Mech. Phys. Solids 73 (2014) 84–102.
[28] F. Guo, D. Zhang, X. Yang, L. Jiang, S. Chai, F. Pan, Mater. Sci. Eng. A 607 (2014) 383–389.
[29] M. Efe, W. Moscoso, K.P. Trumble, W. Dale Compton, S. Chandrasekar, Acta Mater. 60 (2012) 2031–2042.
[30] C. Xu, M.Y. Zheng, K. Wu, E.D. Wang, G.H. Fan, S.W. Xu, S. Kamado, X.D. Liu, G. J. Wang, X.Y. Lv, Mater. Sci. Eng. A 559 (2013) 615–622.
[31] E.O. Hall, Proc. Phys. Soc. B 64 (1951) 747–753.
[32] N.J. Petch, J. Iron Steel Inst. 174 (1953) 25–28.
[33] Y. Guo, M. Efe, W. Moscoso, D. Sagapuram, K.P. Trumble, S. Chandrasekar, Scr. Mater. 66 (2012) 235–238.
[34] L. De Chiffre, Int. J. Mach. Tool Des. Res. 16 (1976) 137–144.
[35] R. Jiang, S. Everitt, M. Lewandowski, N. Gao, P.A.S. Reed, Int. J. Fatigue 62 (2014) 217–227.
[36] S. Nag, P. Sardar, A. Jain, A. Himanshu, D.K. Mondal, Mater. Sci. Eng. A 597 (2014) 253–263.
[37] A.M. Jorge, E. Prokofiev, G. Ferreira de Lima, E. Rauch, M. Veron, W.J. Botta, M. Kawasaki, T.G. Langdon, Int. J. Hydrog. Energy 38 (2013) 8306–8312.
[38] L. Lu, C. Liu, J. Zhao, W. Zeng, Z. Wang, J. Alloy. Compd. 628 (2015) 130–134.
[39] R.Z. Valiev, A.V. Korznikov, R.R. Mulyukov, Mater. Sci. Eng. A 168 (1993) 141–148.
[40] A.I. Almazrouee, K.J. Al-Fadhalah, S.N. Alhajeri, T.G. Langdon, Mater. Sci. Eng. A 641 (2015) 21–28.
[41] W. Moscoso, S. M.R., J.B. Mann, W. Compton, S. Chandrasekar, J. Mater. Res. 22 (2007) 201–205.
[42] G.I. Taylor, Proc. R. Soc. Lond. Ser. A 145 (1934) 362–387.
[43] G.I. Taylor, J. Inst. Met. 62 (1938) 307–325.
[44] V. Shterner, A. Molotnikov, I. Timokhina, Y. Estrin, H. Beladi, Mater. Sci. Eng. A 613 (2014) 224–231.
[45] H. Mecking, U.F. Kocks, Acta Met. 29 (1981) 1865–1875.
[46] L.P. Kubin, Y. Estrin, Acta Metall. Mater. 38 (1990) 697–708.
[47] Y. Estrin, H. Mecking, Acta Met. 32 (1984) 57–70.
[48] J. Liu, Z. Cui, L. Ruan, Mater. Sci. Eng. A 529 (2011) 300–310.
[49] J. Porntadawit, V. Uthaisangsuk, P. Choungthong, Mater. Sci. Eng. A 599 (2014) 212–222.
[50] M.E. Merchant, J. Appl. Phys. 16 (1945) 267–275.
[51] V. Piispanen, J. Appl. Phys. 19 (1948) 876–881.
[52] P.L.B. Oxley, Mechanics of Machining: an Analytical Approach to Assessing Machinability, Wiley, New York, 1989.
[53] R. Komanduri, Appl. Mech. Rev. 46 (1993) 80–132.
[54] M.C. Shaw, Metal Cutting Principles, 2nd ed., Oxford University Press, Oxford, 2005.
[55] F. Khodabakhshi, M. Haghshenas, H. Eskandari, B. Koohbor, Mater. Sci. Eng. A 636 (2015) 331–339.